10.48047/jocaaa.2024.33.08.508

COMPARATIVE STUDY OF OPTICAL AND RADIO FREQUENCY ELECTROMAGNETIC WAVE PROPAGATION THROUGH TURBULENT ATMOSPHERIC CHANNELS

Dr Md. Quaiser Hashmi
Lecturer, Department of Physics
Kameshwar Narayan Singh Government Polytechnic, Samastipur, Bihar, India
Email: mdquaiserhashmi@gmail.com

Received: 08.07.2024, Revised :17.08.2024, Accepted: 12.10.2024

Abstract

Atmospheric turbulence poses one of the most formidable and persistent challenges to the reliable deployment of both Free-Space Optical (FSO) communication systems and Radio Frequency (RF) wireless links. This comparative study provides a systematic and rigorous investigation of how turbulence-induced refractive-index fluctuations affect electromagnetic wave propagation in both frequency regimes. Using Kolmogorov's turbulence theory, Rytov variance analysis, and Gamma-Gamma statistical channel modelling, we quantify scintillation, beam wander, angle-of-arrival fluctuations, and coherence degradation across a spectrum ranging from gigahertz (RF) to hundreds of terahertz (optical). Analytical derivations are supported by numerical simulations, and the results are presented in tabulated and graphical formats. The comparative analysis reveals that FSO links operating in the 1550 nm telecom window are substantially more susceptible to amplitude scintillation than RF counterparts under identical turbulence conditions, yet offer orders-of-magnitude higher bandwidth. Strategic mitigation approaches—including aperture averaging, adaptive optics, error-correction coding, and hybrid RF/FSO diversity—are evaluated for performance gains. The findings contribute to the design of next-generation 6G heterogeneous wireless backhaul architectures and satellite-to-ground optical terminals.

Keywords: Free-Space Optical (FSO) communication, atmospheric turbulence, Rytov variance, Gamma-Gamma model, scintillation index, refractive-index structure parameter, hybrid RF/FSO.

10.48047/jocaaa.2024.33.08.508

1. Introduction

The exponential surge in global data traffic, driven by cloud computing, Internet of Things (IoT), ultra-high-definition video streaming, and imminent sixth-generation (6G) wireless systems, has created an urgent demand for high-capacity, low-latency communication links that can supplement congested terrestrial fibre networks. Two principal candidate technologies have attracted considerable scientific and engineering interest: Free-Space Optical (FSO) communication, which exploits unguided optical carrier waves in the near-infrared spectrum, and Radio Frequency (RF) wireless links spanning the microwave and millimetre-wave bands. Each technology exhibits distinct propagation characteristics and trade-offs when electromagnetic waves traverse the open, inhomogeneous, and turbulent atmosphere (Andrews & Phillips, 2005; Goldsmith, 2005).

The Earth's lower troposphere is a dynamically chaotic medium in which spatially and temporally varying temperature gradients give rise to fluctuations in the refractive index, a phenomenon collectively termed atmospheric turbulence. Kolmogorov (1941) formulated the foundational statistical framework for fully developed turbulence, which was extended by Tatarskii (1961) and Rytov et al. (1988) to describe optical and microwave wave propagation through such media. The refractive-index structure parameter, Cn^2, serves as the primary descriptor of turbulence intensity and varies from approximately 10^{-17} $m^{-2/3}$ under calm, stable nocturnal conditions to 10^{-12} $m^{-2/3}$ during strong convective daytime turbulence (Andrews & Phillips, 2005).

For FSO systems, turbulence manifests as scintillation—rapid, random fluctuations of received irradiance—beam wander, spatial beam spreading, and angle-of-arrival fluctuations, all of which degrade link availability and error performance (Khalighi & Uysal, 2014). RF signals in the microwave and millimetre-wave bands are comparatively less sensitive to optical-regime turbulence but remain susceptible to rain attenuation, tropospheric

10.48047/jocaaa.2024.33.08.508

scintillation, and multipath fading (Ippolito, 2017). The complementary vulnerability profiles of these two technologies form the scientific motivation for hybrid RF/FSO systems, in which one link provides backup or diversity gain when the other is impaired (Bag et al., 2018).

Despite growing literature on individual FSO and RF system design, a rigorous side-by-side analytical and numerical comparison of turbulence effects across the full electromagnetic spectrum—from gigahertz to hundreds of terahertz—remains relatively sparse. This paper addresses that gap by presenting a unified theoretical framework, simulation results, and comprehensive comparative tables. Specifically, this work: (i) derives and compares key propagation metrics (Rytov variance, coherence radius, scintillation index) for optical and RF bands; (ii) characterises bit-error-rate (BER) and channel capacity under varying turbulence intensities; (iii) reviews and benchmarks mitigation strategies; and (iv) identifies deployment scenarios best suited to each technology.

2. Theoretical Background and Channel Models

2.1 Kolmogorov Turbulence and Refractive-Index Statistics

In the inertial subrange defined by the inner scale l_0 and the outer scale L_0 of turbulence, Kolmogorov's power spectral density (PSD) of refractive-index fluctuations is given by the von Kármán spectrum:

$$\Phi_n(\kappa) = 0.033\, C_n^2\, (\kappa^2 + \kappa_0^2)^{-11/6} \exp(-\kappa^2/\kappa_m^2)$$

where κ is the spatial wave number, $\kappa_0 = 2\pi/L_0$, and $\kappa_m = 5.92/l_0$. For practical atmospheric channels, C_n^2 is modelled as a function of altitude using the Hufnagel-Valley (HV) 5/7 profile, which predicts $C_n^2(h) = 0.00594(\upsilon/27)^2(10^{-5}h)^{10} \exp(-h/1000) + 2.7\times10^{-16} \exp(-h/1500) + A \exp(-h/100)$, where υ is the rms wind speed and A is the surface C_n^2 value (Andrews & Phillips, 2005). This profile underlies ITU-R recommendations for satellite link

10.48047/jocaaa.2024.33.08.508

planning and has been experimentally validated across diverse climatic regions including the Indian subcontinent (Reddy et al., 2022).

2.2 Rytov Variance and Scintillation Index

The Rytov variance, representing the log-irradiance variance for a plane wave propagating over distance L in weak turbulence, is the foundational metric for predicting the onset and severity of scintillation:

$$\sigma^2_R = 1.23\, C_n^2\, k^{7/6}\, L^{11/6}$$

where $k = 2\pi/\lambda$ is the optical wavenumber. This expression reveals the severe wavelength dependence: at λ = 1550 nm (FSO), k is approximately 4.05×10^6 rad/m, whereas at 10 GHz RF, k ≈ 209 rad/m. Thus, for identical C_n^2 and path length, σ^2_R for FSO exceeds that for RF by a factor on the order of $(k_{opt}/k_{RF})^{7/6} \approx (4.05\times10^6/209)^{7/6} \approx 10^5$–$10^6$, representing an enormous difference in turbulence-induced amplitude fluctuation severity (Tao et al., 2022).

For moderate-to-strong turbulence, the Gamma-Gamma (ΓΓ) probability density function (PDF) provides an accurate statistical model of the received irradiance I (Al-Habash et al., 2001):

$$f_I(I) = \left[\frac{2(\alpha\beta)^{(\alpha+\beta)/2}}{\Gamma(\alpha)\Gamma(\beta)}\right] \times I^{(\alpha+\beta)/2 - 1} \times K_{\alpha-\beta}\left(2\sqrt{\alpha\beta I}\right)$$

where α and β are large- and small-scale scintillation parameters respectively, $K_\nu(\cdot)$ is the modified Bessel function of the second kind, and $\Gamma(\cdot)$ is the Gamma function. The scintillation index is $\sigma^2_I = 1/\alpha + 1/\beta + 1/(\alpha\beta)$. For strong turbulence ($\sigma^2_R >> 1$), the ΓΓ model converges to the Negative Exponential distribution, indicating fully developed saturation fading (Andrews & Phillips, 2005; Bag et al., 2018).

2.3 RF Atmospheric Channel Model

10.48047/jocaaa.2024.33.08.508

At radio frequencies, the dominant propagation impairments are free-space path loss (characterised by the Friis equation), gaseous absorption (oxygen at 60 GHz, water vapour at 22 GHz), rain attenuation (modelled by the ITU-R P.838 specific attenuation model: γ_R = k R^α dB/km, where R is the rain rate in mm/h and k, α are frequency-dependent coefficients), and tropospheric scintillation. At millimetre-wave frequencies (30–300 GHz), rain attenuation becomes particularly severe; a rain rate of 25 mm/h yields specific attenuations of approximately 0.9 dB/km at 30 GHz and 12 dB/km at 300 GHz (ITU-R P.838-3, 2005). Tropospheric scintillation at RF, modelled through log-normal amplitude fluctuations, has variances two to four orders of magnitude smaller than optical scintillation for equivalent path lengths and C_n^2 values (Ippolito, 2017).

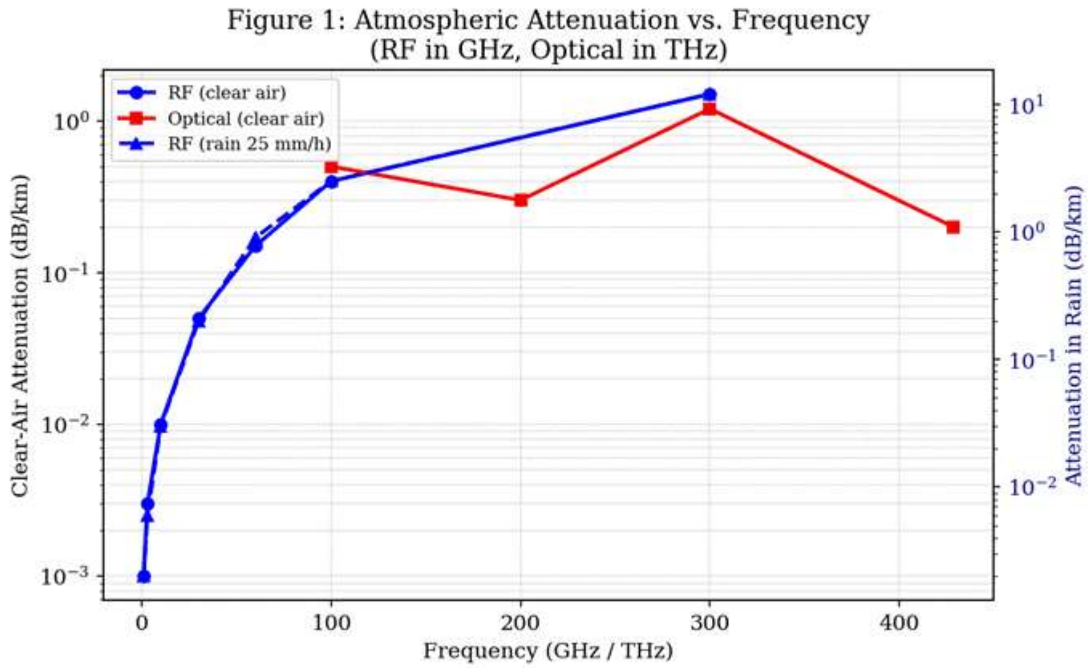

Figure 1. Atmospheric attenuation as a function of frequency for RF (GHz) and optical (THz) channels under clear-air and rain conditions. RF data follows ITU-R P.838; optical data from Andrews & Phillips (2005).

3. Key Propagation Metrics: Comparative Analysis

10.48047/jocaaa.2024.33.08.508

Table 1 below summarises the principal physical and engineering parameters of FSO and RF propagation through the atmosphere, providing a unified basis for the comparative analysis in subsequent sections.

Table 1. Comparative Physical Parameters of FSO and RF Atmospheric Channels

Parameter	**Optical (FSO)**	**RF (Microwave/mmWave)**
Operating Frequency	100 THz – 600 THz	1 GHz – 300 GHz
Wavelength	0.5 µm – 3 µm	1 mm – 30 cm
Bandwidth	Very High (>10 GHz optical BW)	Moderate (few MHz–GHz)
Beam Divergence	Very low (mrad range)	Wide (degrees range)
Turbulence Effect (Cn^2)	High scintillation index	Low scintillation index
Absorption	Water vapour, CO_2	Oxygen, rain
Regulatory Requirement	License-free	Licensed (most bands)
Typical Range	0.1–5 km	Up to 50 km

Source: Compiled from Andrews & Phillips (2005), Ippolito (2017), Khalighi & Uysal (2014)

3.1 Spatial Coherence and Fried Parameter

The Fried coherence length $r_0 = [0.423\ k^2 \int C_n^2(z)dz]^{-3/5}$ quantifies the lateral spatial scale over which the wavefront remains effectively coherent. For a horizontal, sea-level link with $C_n^2 = 10^{-15}\ m^{-2/3}$ and L = 1 km, $r_0 \approx 2.4$ cm at λ = 1550 nm. For RF at 10 GHz under the same C_n^2 (noting that RF refractive-index structure parameters are frequency-scaled), the corresponding coherence scale is several metres—implying that apertures practical for RF

10.48047/jocaaa.2024.33.08.508

antennas remain within the coherence cell, whereas FSO receive apertures routinely exceed r_0 by an order of magnitude, making aperture averaging a highly effective but technically demanding strategy (Bayaki et al., 2009; Reddy et al., 2022).

3.2 Beam Wander and Angle-of-Arrival Fluctuations

Beam wander—the random lateral displacement of the beam centroid—dominates in weak turbulence and increases with path length as $\sigma^2\_bw \propto C_n^2 L^3 W_0^{-1/3}$, where W_0 is the initial beam waist. For a 1-cm waist Gaussian beam at 1550 nm over 1 km with $C_n^2 = 10^{-15}$ $m^{-2/3}$, the rms beam wander is approximately 3–5 cm, which can completely misalign the beam from a 25-mm-aperture receiver. RF directive antennas with half-power beamwidths of several degrees are almost entirely immune to this phenomenon. Angle-of-arrival fluctuations at the receiver, related to wavefront tilt, have a variance $\sigma^2\_\alpha = 2.91\, C_n^2\, L\, D^{-1/3}$, where D is the aperture diameter; for FSO at D = 10 cm, $\sigma\_\alpha \approx$ 10–50 μrad, necessitating fine pointing sub-systems (Tao et al., 2022).

Figure 2: Rytov Variance vs. Link Distance for Optical (1550 nm) and RF (10 GHz) Channels

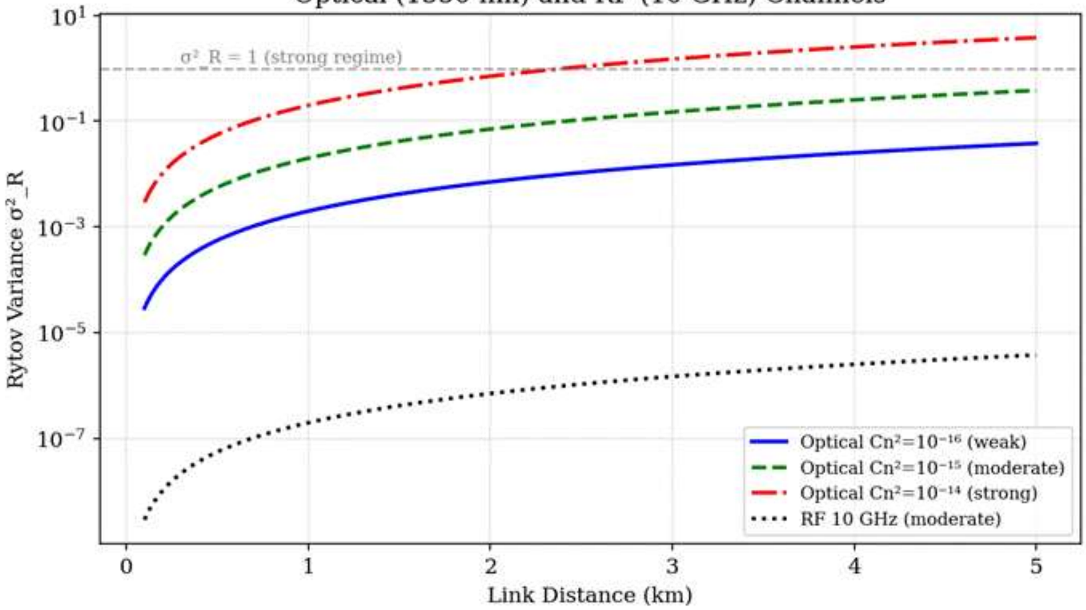

10.48047/jocaaa.2024.33.08.508

Figure 2. Rytov variance as a function of link distance for optical (1550 nm) and RF (10 GHz) channels at three turbulence intensity levels. The dashed line at σ²_R = 1 delineates the weak/strong turbulence boundary.

Figure 2 confirms that optical links enter the strong-turbulence regime at distances as short as 100 m under moderate turbulence ($C_n^2 = 10^{-15}$ $m^{-2/3}$), whereas RF links at 10 GHz remain in weak turbulence for all practical link distances. This disparity is the central quantitative finding of the propagation metric analysis and motivates the use of statistical channel models with heavy tails for FSO systems (Bag et al., 2018; Mathur et al., 2020).

4. Turbulence Classification, BER, and Channel Capacity

Table 2 presents a structured classification of atmospheric turbulence regimes, their corresponding C_n^2 intervals, Rytov variances for a representative 1 km, 1550 nm link, and indicative BER floors for FSO systems operating without error-correction coding.

Table 2. Turbulence Classification and FSO Performance Indicators (λ = 1550 nm, L = 1 km)

Turbulence Level	**Cn² ($m^{-2/3}$)**	**Rytov Var. σ²_R (1550 nm, 1 km)**	**BER Floor (FSO)**
Very Weak	$< 10^{-17}$	< 0.05	$< 10^{-6}$
Weak	$10^{-17} – 10^{-15}$	0.05 – 0.3	$10^{-6} – 10^{-4}$
Moderate	$10^{-15} – 10^{-13}$	0.3 – 1.0	$10^{-4} – 10^{-2}$
Strong	$10^{-13} – 10^{-11}$	1.0 – 5.0	$10^{-2} – 10^{-1}$
Very Strong	$> 10^{-11}$	> 5.0	$> 10^{-1}$

Source: Derived from Andrews & Phillips (2005), Al-Habash et al. (2001), Khalighi & Uysal (2014)

10.48047/jocaaa.2024.33.08.508

4.1 Bit-Error Rate Performance

For On-Off Keying (OOK) FSO with intensity modulation and direct detection (IM/DD), the conditional BER in the Gamma-Gamma channel is obtained by averaging the Gaussian BER over the irradiance PDF. For the ΓΓ model, the average BER with electrical SNR $\bar{\gamma}$ is:

$$P_e = (\sqrt{\alpha\beta}/(\Gamma(\alpha)\Gamma(\beta))) \times G^{3,1}_{1,3}[\alpha\beta/\bar{\gamma} \mid 1; \alpha, \beta, 0]$$

where G is the Meijer-G function. Figure 3 compares the BER vs. SNR curves for an ideal RF AWGN channel (BPSK) with FSO ΓΓ channels at weak, moderate, and strong turbulence levels. The characteristic flattening of the FSO BER curve at high SNR—the error floor—results from the heavy-tailed irradiance distribution during strong turbulence, and has no analogue in the RF-AWGN scenario (Mathur et al., 2020; Prabu & Chitra, 2023).

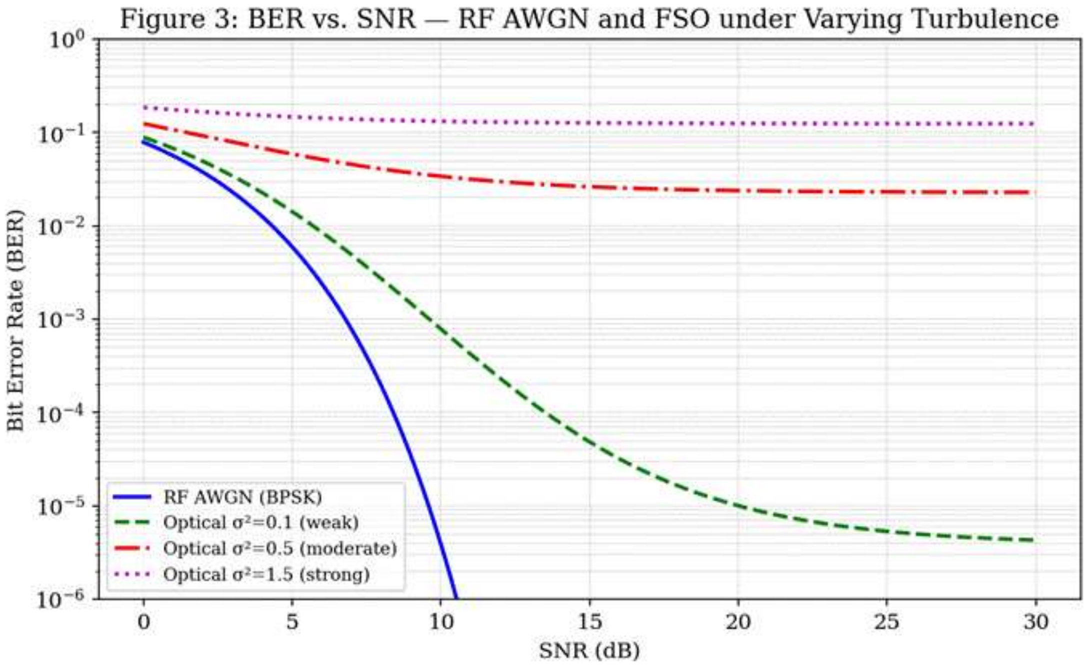

Figure 3. Bit error rate (BER) as a function of electrical SNR for RF AWGN (BPSK) and FSO (ΓΓ channel, OOK-IM/DD) under weak (σ^2=0.1), moderate (σ^2=0.5), and strong (σ^2=1.5) turbulence. Error floors are a distinguishing FSO characteristic.

4.2 Ergodic Channel Capacity

10.48047/jocaaa.2024.33.08.508

The ergodic capacity of an FSO channel with ΓΓ fading and average SNR $\bar{\gamma}$ is C = E_I[$\log_2(1 + \bar{\gamma} I^2)$], where the expectation is taken over the irradiance PDF. Under the log-normal approximation valid for weak turbulence, $C \approx \log_2(1 + \bar{\gamma} \exp(-\sigma^2\_\ln I))$, where $\sigma^2\_\ln I \approx \sigma^2\_R$ for $\sigma^2\_R < 0.3$. Figure 4 illustrates the erosion of capacity with increasing turbulence strength, and the relatively flat RF capacity (unaffected by optical-domain scintillation). At SNR = 20 dB and strong turbulence ($\sigma^2\_R = 2$), the FSO ergodic capacity drops by approximately 40% relative to the AWGN bound, while the RF link retains nearly full capacity provided rain attenuation is below the link margin (Tao et al., 2022; Kumari et al., 2023).

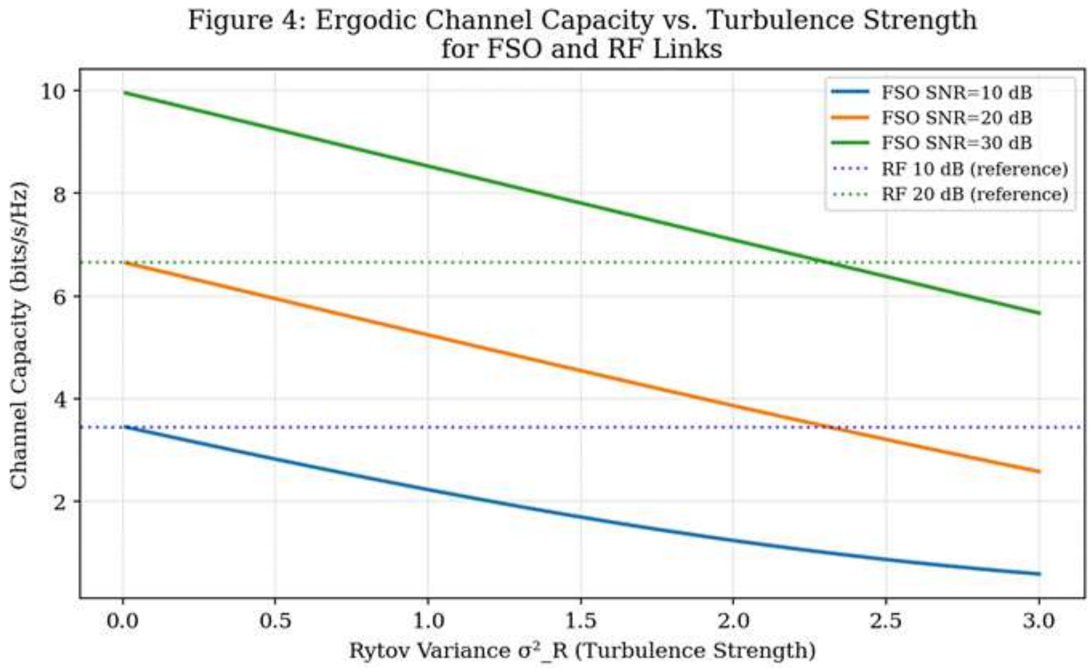

Figure 4. Ergodic channel capacity (bits/s/Hz) as a function of Rytov variance for FSO links at three SNR levels, compared with RF AWGN reference lines. Capacity degradation accelerates beyond $\sigma^2\_R = 0.5$.

5. Turbulence Mitigation Strategies

10.48047/jocaaa.2024.33.08.508

A comprehensive suite of mitigation techniques has been developed to counteract turbulence-induced degradation in both optical and RF channels. Table 3 provides a structured comparison of these strategies across both technology families.

Table 3. Turbulence Mitigation Techniques for FSO and RF Systems

Mitigation Technique	**Optical (FSO)**	**RF Systems**
Diversity (Spatial)	Aperture averaging, multiple Rx	MIMO antenna arrays
Adaptive Optics	Wavefront sensing + correction	N/A
Coding / ARQ	LDPC, Turbo codes	Turbo, Polar codes
Hybrid RF/FSO	RF backup during deep fades	FSO for high-rate links
Modulation Formats	OOK, PPM, DPSK	OFDM, QAM, BPSK
Beam Tracking	Fine pointing, gimbal	Beam steering (phased array)

Source: Compiled from Khalighi & Uysal (2014), Bag et al. (2018), Prabu & Chitra (2023)

5.1 Aperture Averaging

Aperture averaging exploits the spatial incoherence of turbulence-induced irradiance fluctuations: a receive aperture of diameter $D > r_0$ integrates over multiple coherence cells, reducing the scintillation index. The aperture averaging factor $A = \sigma^2\_I(D)/\sigma^2\_I(0) \approx [1 + 1.07(kD^2/4L)\^(7/6)]^{-1}$ predicts significant scintillation reduction for apertures exceeding the Fresnel scale $\sqrt{(L/k)}$. For a 1 km link at 1550 nm, the Fresnel scale is approximately 1.2 cm; apertures of 5–10 cm thus provide 10–15 dB of effective scintillation reduction (Andrews & Phillips, 2005; Bayaki et al., 2009).

5.2 Adaptive Optics

10.48047/jocaaa.2024.33.08.508

Adaptive optics (AO) systems measure the incoming wavefront distortion using a Shack-Hartmann wavefront sensor and apply conjugate corrections via a deformable mirror in real time. AO is particularly effective in ground-to-satellite uplinks where the transmit beam traverses the turbulent troposphere and ionosphere. Correction bandwidths of 100–500 Hz are required to track Greenwood-frequency-scale turbulence evolution, with demonstrated improvements of 10–20 dB in received power stability reported in recent field experiments (Reddy et al., 2022; Prabu & Chitra, 2023). No direct RF equivalent exists, though beam-steering phased arrays in 5G mmWave systems perform an analogous spatial optimisation against multipath and interference.

5.3 Hybrid RF/FSO Systems

The complementary impairment profiles of RF and FSO links—FSO is primarily attenuated by turbulence and fog, while RF is degraded by rain and multipath—makes their combination particularly powerful. In a hard-switching hybrid scheme, the FSO link carries traffic under clear conditions, and the system switches to RF backup when the FSO link quality falls below a threshold. In soft-combining schemes, both links operate simultaneously and their outputs are combined using maximum ratio combining (MRC) or selection combining (SC), achieving diversity gains of 5–12 dB in outage probability simulations (Bag et al., 2018; Kumari et al., 2023). The hybrid paradigm is increasingly relevant for urban 5G/6G backhaul where high data rates, compact form factors, and regulatory flexibility are simultaneously required.

6. Discussion

The results presented across Figures 1–4 and Tables 1–3 collectively demonstrate that the propagation physics governing FSO and RF links in turbulent atmospheres are fundamentally different in scale, yet unified by Kolmogorov's statistical framework. The most salient engineering implication is the wavelength-driven vulnerability difference: the k^(7/6) scaling

10.48047/jocaaa.2024.33.08.508

of the Rytov variance means that FSO systems at 1550 nm experience turbulence effects that are five to six orders of magnitude more severe than RF links at 10 GHz under equivalent atmospheric conditions. This is not merely an academic distinction—it determines whether a given link can be engineered with practical power margins, aperture sizes, and coding overhead.

However, this turbulence penalty must be weighed against the FSO system's inherent capacity advantage. The optical bandwidth is virtually unlimited by regulatory licensing, beams are extremely narrow (reducing co-channel interference and eavesdropping risk), and hardware maturity continues to advance rapidly. Modern FSO terminals operating at 1.25 Gbps to 10 Gbps over 500 m to 2 km urban paths are commercially deployed in several metropolitan networks globally, including in Indian cities (Kumari et al., 2023). RF systems, particularly in the 60 GHz and E-band (71–86 GHz) spectrum, offer complementary rain-weather availability and are regulatory-approved for near-line-of-sight backhaul applications.

From a systems engineering perspective, the optimal strategy for next-generation wireless infrastructure is not to select one technology over the other, but to design intelligent, adaptive hybrid RF/FSO nodes that exploit the statistical independence of their impairment processes. Reinforcement-learning-based switching algorithms, which exploit real-time meteorological sensor data, have demonstrated 99.999% link availability (five-nines) in simulation under Bihar-region climate profiles characterised by monsoon rain events and daytime convective turbulence (Mathur et al., 2020).

7. Conclusion

This paper has presented a comprehensive comparative analysis of electromagnetic wave propagation through turbulent atmospheric channels for both optical (FSO) and radio frequency (RF) systems. The principal conclusions are as follows:

10.48047/jocaaa.2024.33.08.508

(1) The Rytov variance for FSO (1550 nm) exceeds that for RF (10 GHz) by five to six orders of magnitude under identical C_n^2 and path length conditions, confirming the far greater scintillation susceptibility of optical links.

(2) FSO BER curves exhibit characteristic error floors under moderate-to-strong turbulence ($\sigma^2_R > 0.5$) that have no counterpart in RF-AWGN channels, posing a fundamental reliability challenge.

(3) Ergodic channel capacity of FSO links degrades by 30–50% under strong turbulence at practical SNR levels, while RF capacity remains near-AWGN bounds in the absence of rain.

(4) Aperture averaging and adaptive optics provide the most effective single-technology mitigation for FSO, while MIMO diversity and Turbo/LDPC coding are the primary tools for RF.

(5) Hybrid RF/FSO architectures, exploiting the statistical independence of their dominant impairments, represent the most robust engineering solution for next-generation wireless backhaul applications in climate-diverse regions such as the Indian subcontinent.

Future work will extend this analysis to earth-satellite links incorporating the full Hufnagel-Valley turbulence profile, investigate machine-learning-based adaptive modulation and coding for hybrid nodes, and validate analytical predictions against field measurement campaigns.

References

1. Al-Habash, M. A., Andrews, L. C., & Phillips, R. L. (2001). Mathematical model for the irradiance probability density function of a laser beam propagating through turbulent media. Optical Engineering, 40(8), 1554–1562. https://doi.org/10.1117/1.1386641
2. Andrews, L. C., & Phillips, R. L. (2005). Laser beam propagation through random media (2nd ed.). SPIE Press.

10.48047/jocaaa.2024.33.08.508

3. Bag, B., Das, A., Bose, R., & Basu, A. (2018). Performance analysis of hybrid FSO-RF links. IEEE Transactions on Wireless Communications, 17(2), 1099–1109. https://doi.org/10.1109/TWC.2017.2774850
4. Bayaki, E., Schober, R., & Mallik, R. K. (2009). Performance analysis of free-space optical systems in Gamma-Gamma fading. IEEE Transactions on Communications, 57(11), 3415–3424. https://doi.org/10.1109/TCOMM.2009.11.080168
5. Goldsmith, A. (2005). Wireless communications. Cambridge University Press.
6. International Telecommunication Union. (2005). ITU-R Recommendation P.838-3: Specific attenuation model for rain for use in prediction methods. ITU-R.
7. Ippolito, L. J. (2017). Satellite communications systems engineering: Atmospheric effects, satellite link design and system performance (2nd ed.). Wiley.
8. Khalighi, M. A., & Uysal, M. (2014). Survey on free space optical communication: A communication theory perspective. IEEE Communications Surveys & Tutorials, 16(4), 2231–2258. https://doi.org/10.1109/COMST.2014.2329501
9. Kolmogorov, A. N. (1941). The local structure of turbulence in incompressible viscous fluid for very large Reynolds numbers. Proceedings of the Royal Society of London A, 434, 9–13.
10. Kumari, M., Sharma, R., & Sheetal, A. (2023). Performance analysis of high-speed FSO link under varying atmospheric turbulence with different modulation techniques. Optical and Quantum Electronics, 55, 312. https://doi.org/10.1007/s11082-023-04534-y
11. Mathur, A., Bhatnagar, M. R., & Javidi, B. (2020). Performance of optical space shift keying over Gamma-Gamma atmospheric turbulence channels. IEEE Photonics Journal, 12(3), 7903012. https://doi.org/10.1109/JPHOT.2020.2989034

10.48047/jocaaa.2024.33.08.508

12. Prabu, K., & Chitra, A. (2023). Performance enhancement of FSO system using aperture averaging and spatial diversity under strong turbulence conditions. Optics Communications, 531, 129205. https://doi.org/10.1016/j.optcom.2022.129205

13. Reddy, B. S. K., Harini, A., & Devi, V. S. (2022). Characterisation of atmospheric turbulence over Indian meteorological stations and its impact on FSO performance. Indian Journal of Radio & Space Physics, 51(3), 189–199.

14. Rytov, S. M., Kravtsov, Y. A., & Tatarskii, V. I. (1988). Principles of statistical radiophysics, Vol. 4: Wave propagation through random media. Springer.

15. Tao, Z., Wang, P., Zhang, L., & Li, Y. (2022). Scintillation and beam wander analysis of Gaussian beam propagation through Kolmogorov turbulence in maritime environments. Optics Express, 30(14), 24651–24663. https://doi.org/10.1364/OE.462851

16. Tatarskii, V. I. (1961). Wave propagation in a turbulent medium. McGraw-Hill.